ADVANCED FUNCTIONAL MATERIALS

www.afm-journal.de

# UV-Induced Multilevel Current Amplification Memory Effect in Zinc Oxide Rods Resistive Switching Devices

*Paola Russo, Ming Xiao, Robert Liang, and Norman Y. Zhou**

**Zinc oxide (ZnO) devices represent an alternative in the semiconductor technology for their application in resistive switching memory devices and ultraviolet (UV) photodetectors due to their chemical and electrical properties. The multilevel current amplification of ZnO rods RRAM devices induced by UV light illumination is reported here for the first time. The resistive switching mechanism underlying in this type of devices is attributed to the formation of conductive filaments composed of oxygen vacancies. The analysis of the photodecay processes carried out on the devices fabricated with different electrodes shows that the type of interface (Ag/ZnO and Au/ZnO) affects the surface barrier height, which influences the photodecay rate. It is shown that by applying UV light, higher relaxation constants (slower photodecay rates) are obtained and lead to multilevel current amplification behavior.**

## 1. Introduction

ZnO nanostructures have been intensively researched as they are considered alternatives to traditional semiconductors for future nonvolatile memory technology[1,2] and optoelectronics.[3–5] The interest in theses nanomaterials is due to their outstanding properties such as their transparency in the visible region, low cost, wide direct bang gap (3.34 eV), and chemical stability. Many studies have focused on the synthesis of ZnO rods for the fabrication of resistive switching (RS) random access memory (RRAM).[6–13] These devices consist of an active layer sandwiched between two metallic electrodes and rely on the resistance change of the active material under application of an electrical stimulus, from a low resistance state (LRS or "ON") to a high resistance state (HRS or "OFF") and vice versa.[14–17] When a device is switched from HRS to LRS, the process is referred as the SET, while the RESET is the process of switching the device from LRS to HRS. Different types of RRAM devices have been fabricated using materials with various morphologies and one of the advantages of using ZnO in RRAM devices is the possibility of growing ZnO with numerous morphologies, which span from nanowires, nanorods, to nanofilms and nanoparticles. This diversity of nanostructures along with the outstanding properties of ZnO, such as its biocompatibility, controllable electrical behavior, and ecofriendliness, make this material a promising candidate for the development of various RRAM structures.[10,18] Moreover, ZnO has a great potential to be employed for the fabrication of light emitting diodes and UV photodetectors.[4,19–23] The understanding of the mechanism underlying the RS behavior in these type of RRAM devices or the study of the photoconductive response (a key parameter in a photoconductor) are essential for the control and engineering of ZnO-based devices.[4] In ZnO RRAM devices, depending on the device's structure, RS effect can operate under unipolar and bipolar operation mode, where the SET and RESET processes occurs in the same or opposite bias polarity, respectively.[1,2] The resistive switching behavior underlying ZnO based RRAM can be attributed to the electrochemical metallization mechanism induced by the formation and rupture of metallic filaments or to the valence change mechanism where the conductive filaments are composed of oxygen vacancies defects.[10] Several studies have reported that oxygen vacancies play a key role not only in the mechanism of RS[10] but as well in UV photodetector performances.[21,22,24–26] Upon applying voltage, oxygen vacancies will form conductive filaments responsible for RS behavior;[10] upon illumination of UV light, they act as hole-trapping sites at the ZnO surface. The photogenerated holes are trapped at the hole trapping states increasing the lifetime of the photogenerated electrons leading to photoconductive gain.[24,27,28] So far, reports on ZnO nanostructures for optoelectronics have focused on the improvement of the photodetectors by mixing the ZnO with other materials such as carbon nanodots,[29] gold nanoparticles,[30] cadmium sulfide films,[31] and so on. Fewer studies have been carried out on the study of the effect of UV irradiation of ZnO RRAM,[32] which require further investigation in order to improve and engineer the performance of next-generation RRAM devices.

In this work we investigated the multilevel current amplification of ZnO rods RRAM device upon illumination with UV light, which is the first study of its kind. Multilevel cells are attracting growing interest for the possibility of storing more than one-bit per cell having more than two resistance states.[10,33,34] Despite the explanation of the origin of multilevel behavior in RRAM devices is under debate, different hypothesis have been elaborated. In particular, accumulations of defects which can vary the size of the conductive filaments, modification of the depletion layer which modify the barrier height,

Dr. P. Russo, M. Xiao, Dr. R. Liang, Prof. N. Y. Zhou
Department of Mechanical and Mechatronics Engineering
Centre for Advanced Materials Joining (CAMJ)
Waterloo Institute for Nanotechnology (WIN)
University of Waterloo
200 University Avenue West Waterloo, Ontario N2L 3G1, Canada
E-mail: nzhou@uwaterloo.ca

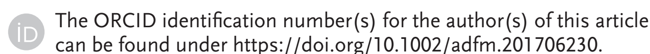
The ORCID identification number(s) for the author(s) of this article can be found under https://doi.org/10.1002/adfm.201706230.

**DOI: 10.1002/adfm.201706230**


© 2018 WILEY-VCH Verlag GmbH & Co. KGaA, Weinheim

or controlling the current compliance have been proposed as explanation for the multilevel behavior.[10,35–37] The study was carried out investigating the electrical performances of the ZnO rod device in dark and under UV irradiation. The device showed bipolar resistive switching behavior originated by oxygen vacancies, and the stability of RS behavior is improved by UV illumination. A current amplification of the ZnO device was observed under UV light, which was not observed in dark conditions. From the preliminary results obtained, a possible RS mechanism is proposed along with hypothesis to explain the current amplification behavior upon UV exposure of the device.

## 2. Results and Discussion

The ZnO rods were synthesized by a two-step electrochemical deposition process. The advantages of electrophoretic deposition is its cost- and time-effectiveness when compared to hydrothermal and sol–gel synthesis routes.[38–40] The ZnO rods fabrication procedure is described in detail in the Experimental Section. In short, the ZnO rods were synthesized in two steps in a three-electrode quartz cell using the fluorine doped tin oxide (FTO) substrate as working electrode and Pt mesh as counter electrode. The first step of the rods' growth involved the synthesis of the ZnO seed layer applying a cathodic potential in a solution of zinc nitrate hexahydrate [$Zn(NO_3)_2 \cdot 6 H_2O$]. In the second and final step, the growth of the ZnO rods was achieved through the application of a cathodic potential in a equimolar solution of $Zn(NO_3)_2$ and hexamethylenetetramine (HMTA). The mechanism for the growth of the ZnO rods thorough electrophoretic deposition has been well reported and it is attributed to the reaction between the $Zn^{2+}$ ions, dissolved in the growth solution, with hydroxide ($OH^-$) ions generated upon application of an electric field. The reactions involved in the growth of the ZnO rods can be described as follows

$$Zn(NO_3)_2 \rightarrow Zn^{2+} + 2NO_3^- \quad (1)$$

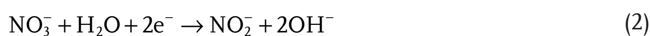

$$NO_3^- + H_2O + 2e^- \rightarrow NO_2^- + 2OH^- \quad (2)$$

$$Zn^2 + OH^- \rightarrow Zn(OH)_2 \quad (3)$$

$$Zn(OH)_2 \rightarrow ZnO + H_2O \quad (4)$$

The HMTA reacting with water provides additional hydroxide ions according to the following reactions[3,41,42]

$$C_6H_{12}N_4 + 6H_2O \rightleftarrows COH_2 + 4NH_3 \quad (5)$$

$$NH_3 + H_2O \rightleftarrows NH_4^+ + OH^- \quad (6)$$

The morphology and the structure of the ZnO rods were analyzed by scanning electron microscopy (SEM) and transmission electron microscopy (TEM).

**Figure 1**a, shows the top SEM image of the ZnO rods on a seeded FTO substrate, while a magnified SEM image of the rods is displayed in Figure 1b.

It was possible to obtain a homogenous layer of ZnO rods with an average length of ≈1 µm using solely cathodic deposition. In Figure 1c,d, TEM images of the ZnO rods are displayed. The inset of Figure 1c depicts the selected area electron diffraction (SAED) pattern of the ZnO rods, which confirms their single crystalline structure. The high resolution TEM (HR-TEM) image in Figure 1d, reveals the lattice fringes with d spacing of 0.26 nm, which matches the interspacing of the (002) planes in wurtzite structure, thus confirming the growth direction of the ZnO rods is in the *c*-axis direction.[43,44]

**Figure 2**a displays the Raman characterization analysis of the ZnO rods. The main characteristic peaks of zinc oxide rods are associated to different vibrational modes. In particular, the peak at 379 $cm^{-1}$ corresponds to $A_1$, while $E_1$ originates the peak at 410 $cm^{-1}$. The other two Raman active modes are the low frequency $E_2$ phonon mode originated from the Zn vibrations, and the peak at 437 $cm^{-1}$, which corresponds to the high frequency $E_2$ mode due to oxygen atoms in the structure.[45–47] It has been reported that the position of the $E_2$ (high) mode shifts toward lower frequencies as the amount of oxygen vacancies increases.[48]

The position of the $E_2$ (high) peak in the Raman spectrum displayed in Figure 2a is shifted at lower frequencies located at 435 $cm^{-1}$, suggesting the presence of oxygen vacancies within the ZnO structure. X-ray photoelectron spectroscopy (XPS) analysis was performed in order to analyze the chemical composition and oxidation state of the ZnO rods. The high-resolution spectra of Zn 2p and O1s are shown in Figure 2b,c, respectively. The two peaks located at 1021.51 and 1044.59 eV are attributed to Zn $2p^{3/2}$ and Zn $2p^{1/2}$ of ZnO rods, which indicates a +2 valence state of the rods. Moreover, both the peaks were fitted to a single one Gaussian curve and the binding energy difference between the two Zn 2p core levels is 23 eV, which is in agreement with the data reported in literature for ZnO rods.[11,49,50] The presence of oxygen vacancies and interstitial oxygen defects can be investigated through the chemical state of O 1s region.[11,51,52] In Figure 2c, the spectrum of the O 1s region is displayed and the peak was fitted to three Gaussian peaks located at (i) 530.25, (ii) 531.29, and (iii) 532.10 eV. The peaks at the low and middle binding energies are attributed to $O^{2-}$ ions in the Zn—O bonding in the ZnO rods wurtzite structure and to the $O^{2-}$ ions in the oxygen deficient regions, respectively. The peak at higher binding energy is associated to chemisorbed oxygen. The very strong intensity of the peak at lower binding energy compared to the other two components indicates crystallinity in the samples, as further confirmed by the SAED pattern in the inset of Figure 1c and by the sharp and higher intensity of the $E_2$ (high) Raman peak in Figure 2a.[46,51] The intensity of the peaks located at medium and high binding energies is comparable, indicating the coexistence of oxygen vacancies $V_o$ and chemisorbed oxygen, and is in agreement with previous reports.[51,52]

In order to study the electrical performances of the ZnO rods, silver (Ag) contacts were fabricated (See Experimental Section for details). A schematic of the Ag/ZnO rods/FTO device is displayed in **Figure 3**a,b as insets.

The electrical measurements were performed applying a sweeping voltage of 4 V at the Ag top electrode, while the FTO was grounded. The electrical tests were carried in dark


© 2018 WILEY-VCH Verlag GmbH & Co. KGaA, Weinheim

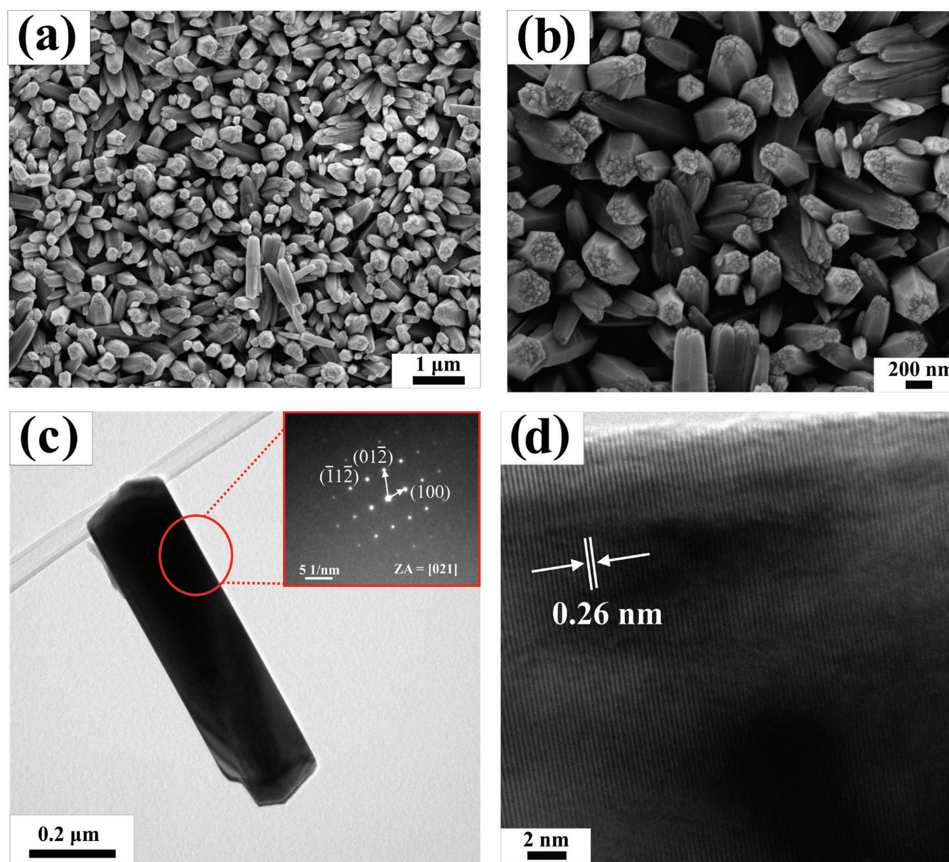


**Figure 1.** a) SEM image of ZnO top surface, b) magnification of the ZnO rods obtained upon cathodic deposition, c) TEM image of ZnO rods showing good crystallinity demonstrated by SAED analysis (inset), d) HR-TEM showing the d spacing of the ZnO rods.

and under UV irradiation and the *I–V* curves are displayed in Figure 3a,b, respectively. Under dark conditions the device showed a bipolar resistance switching, and the device was not stable as current decrease occurred after 40 sweeping cycles. The sweeping direction was 0→4 V→0→−4 V, and it was found that the device was initially in the HRS and switched to the LRS during the voltage sweeping from 4 to 0 V, due to the piling of oxygen vacancies, which creates the conductive filaments, as discussed later. The *I–V* curve of the Ag/ZnO rods/FTO device under UV irradiation (inset Figure 3b) is displayed in Figure 3b, and the illumination conditions changed the electrical response. In particular, an increase of the measured current was observed together with the improvement of the device's stability, which could sustain up to 40 sweeping cycles. The measured current under UV exposure was 20 times greater than the current in dark conditions. The increase of the conductivity of the Ag/ZnO rods/FTO device upon illumination is showed in Figure 3b. ZnO is a n-type semiconductor extremely sensitive to the UV irradiation, and the mechanism for the photoconduction in the nanostructured ZnO has been extensively studied.[21,22,24,25,32] It is well known that in air, oxygen molecules chemisorb on the side surfaces of ZnO rods and, by capturing the free electrons from the n-type ZnO conduction band, are converted to oxygen ions according to the following reaction

$$O_{2(g)} + e^- \rightarrow O^-_{2(ad)} \quad (7)$$

Consequently a low-conductivity depletion layer is formed on the side surfaces of ZnO rods . When the ZnO is illuminated by UV irradiation with photon energies above the semiconductor band gap, electron–hole pairs are photogenerated according to Equation (8)

$$h\nu \rightarrow e^- + h^+ \quad (8)$$

The photogenerated holes react with the oxygen ions releasing oxygen molecules (Equation (9))

$$O^-_{2(ad)} + h^+ \rightarrow O_{2(g)} \uparrow \quad (9)$$

As a consequence the high-resistance depletion layer is reduced and the unpaired electrons, left behind by the photogenerated holes, increase the conductivity under an applied field.[21,22,24,32,52] The bipolar RS behavior of the Ag/ZnO rods/FTO device and the increase of the device's stability upon UV exposure can be explained by the oxygen vacancies conduction mechanism.[11,22,32,52] ZnO possesses intrinsic defects, i.e., oxygen vacancies $V_o$, and the presence of these type of defects in our device has been confirmed by XPS analysis shown in Figure 2c, where the peak at 531.29 eV is associated with $O^{2-}$ ions in the oxygen deficient regions.[52,53] Oxygen vacancies are homogeneously distributed in the ZnO nanostructure (**Figure 4**a), and they can be found in three different charge


© 2018 WILEY-VCH Verlag GmbH & Co. KGaA, Weinheim

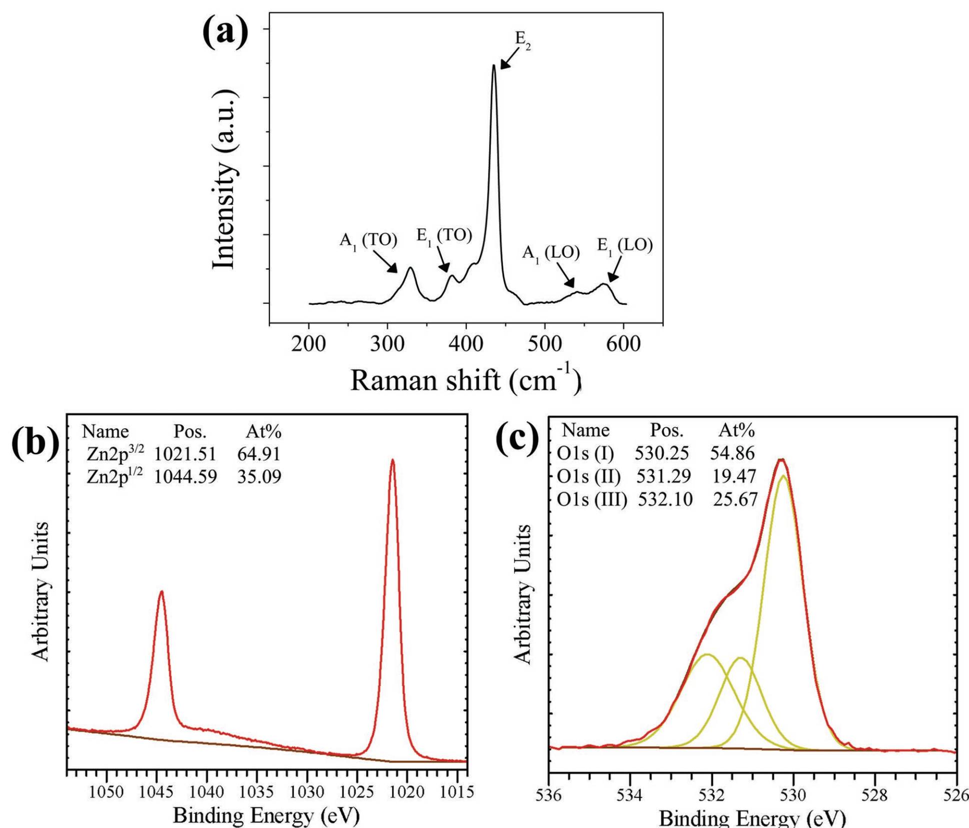


**Figure 2.** a) Raman spectrum; b) Zn 2p core levels and c) O1s region of the as-grown ZnO rods.

states: $V_o$, $V_o^{\cdot}$ and $V_o^{\cdot\cdot}$, where $V_o$ and $V_o^{\cdot}$ act as traps, capturing two and one electrons, respectively.

$V_o^{\cdot}$, and $V_o^{\cdot\cdot}$ are singly and doubly positively charged and drift toward the cathode, while at the anode the charged oxygen vacancies and oxygen ions are produced according to the following reactions

$$O_o \rightarrow V_o^{\cdot\cdot} + 2e^- + \frac{1}{2}O_{2(g)} \quad (10)$$

$$\frac{1}{2}O_{2(g)} \rightarrow O_2^- + 2h^+ \quad (11)$$

Upon application of an electric field, the charged oxygen vacancies will move toward the cathode (FTO bottom electrode). The piling up of the oxygen vacancies from the anode to the cathode originates the conductive filaments responsible of the resistance switching of the device from HRS to LRS, as shown in Figure 4b. At reverse bias the neutral oxygen vacancies ($V_o$) become doubly positively charged after losing their two electrons and the recombination with the oxygen ions ($O_2^-$) takes place, which corresponds to absorption of oxygen. Consequently, the conductive filaments are broken switching the device from LRS to HRS (Figure 4d).[11,54,55] The *I–V* curves of the device exposed to UV light showed an increase of

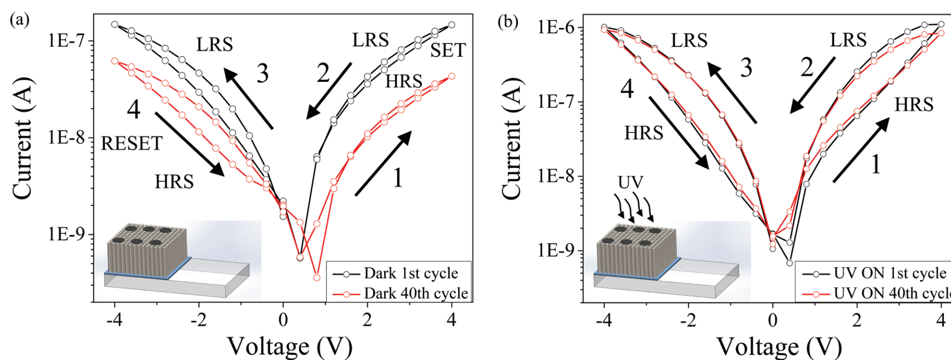


**Figure 3.** a) *I–V* curves of the Ag/ZnO rods/FTO (inset) in dark condition and b) under UV irradiation with a sweeping voltage of 4 V for 1 cycle (black curves) and after 40 cycles (red curves).


© 2018 WILEY-VCH Verlag GmbH & Co. KGaA, Weinheim

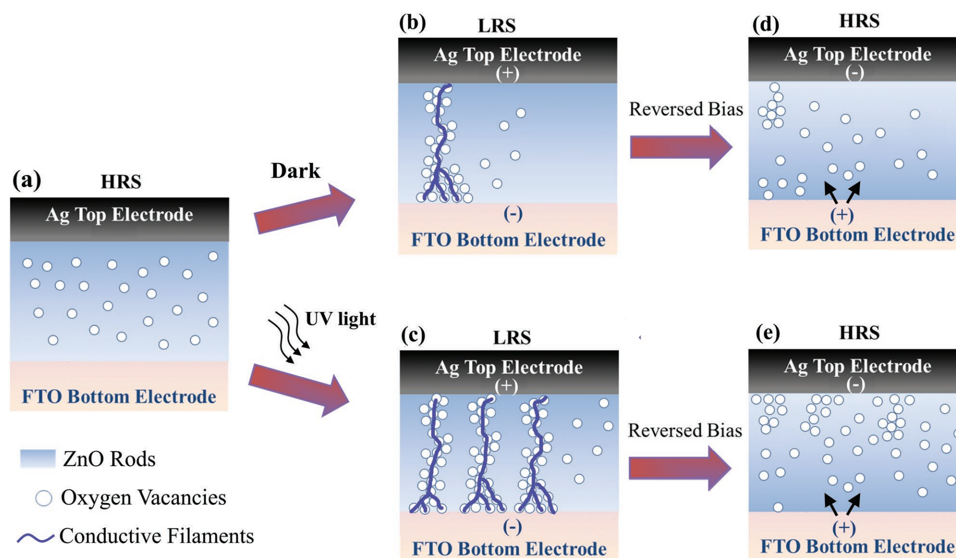


**Figure 4.** Resistive switching mechanism of the Ag/ZnOrods/FTO device. a) Initially the device is in the HRS, upon application of an electric field the oxygen vacancies start to pile up b) and form conductive filaments, which switch the device to LRS. Under UV light illumination c) more oxygen vacancies are formed, which lead to the formation of multiple conductive filaments. At reversed bias d,e), the conductive filaments are broken and the device returns into the OFF state.

stability compared to the ones obtained in the dark, which may be attributed to the higher production of oxygen defects and oxygen ions obtained during UV illumination.[56,57] It has been reported that under UV illumination of ZnO oxygen vacancies will be generated,[56–59] therefore higher amount of oxygen vacancies will be created in the illuminated device compared to the one in dark conditions. The oxygen vacancies drift toward the cathode and start to connect with each other forming multiple conductive filaments (Figure 4c), which are responsible of increase stability of the device.[21,22,24,32,52]

In **Figure 5**, the *I–V* curves of the Ag/ZnO rods/FTO device upon application of consecutive biasing of 4 V under dark conditions and continuous UV irradiation are shown. Under UV illumination (Figure 5a) the device showed a three-level memory current amplification. When a reverse erase bias of –6 V is applied the device goes back to its original state, allowing a repeatable 3 level current amplification. We can ascribe the multilevel current amplification of the ZnO device as a consequence of the multiple conductive paths created under UV light, which increases the number of oxygen vacancies. Indeed, it has been reported that the current amplification is due to the accumulation of charged defects (oxygen vacancies in our devices).[37] The multilevel current amplification is not occurring under dark conditions (Figure 5b). Additionally, at each level the current is constant and the value of current reached is ≈0.06 µA and decreased with the number of cycles. Under UV light, the current reached ≈4 µA, which is two orders of magnitude larger than the one in the dark. The current values for each cycle are reproducible and stable. Despite the fact that the memory current amplification behavior in RRAM devices made from oxide nanomaterials is well known, it has not been reported to occur in ZnO rods, as demonstrated from the results obtained under dark condition (Figure 5b).[60,61]

In dark conditions a low conductive depletion layer is formed near the side surfaces of ZnO rods because the oxygen molecules adsorbed on the ZnO surface are transformed to oxygen ions by capturing free electrons from the n-type ZnO rods, (Equation (7)). However, when the ZnO rods are exposed to UV light, electron–hole pairs are photogenerated (Equation (8)), which leads to a rapid rate of increase in the current. The photogenerated holes discharge the adsorbed oxygen ions on the rod side surfaces and the oxygen is desorbed leading to a decrease of the depletion layer width and to the increase of the current (Equation (9)). When the UV light is turned off, an increase of the depletion layer's width occurs and the current value will reach the initial value of the dark current. The photoresponse rate depends on the concentration of surface defects, surface captured oxygen and on the recombination rate of photogenerated electrons–holes pairs, which are separated by the surface barrier originated by the depletion layer. The lower concentration and lower barrier height leads to a faster photorecombination and therefore faster photoresponse decay.[22,62,63] In order to investigate the photoresponse time of our devices, we applied a constant positive and negative voltage of 1 V to the Ag electrode while the FTO is grounded, and we exposed the device to the UV light for 50 min. In **Figure 6**a,b the photoresponse performances of the device under positive (a) and negative (b) voltage are shown.

The photodecay process can be fitted with the following exponential relaxation equation

$$I = I_0 + Ae^{-\frac{t}{\tau_1}} + Be^{-\frac{t}{\tau_2}} \quad (12)$$

where the two relaxation time constants are indicated as $\tau_1$ and $\tau_2$. These relaxation time constants highlight the presence of two different mechanisms during the decay process, as reported in literature.[22,64] The time constant $\tau_1$ is related the band-to-band recombination in the bulk, while $\tau_2$ depends on the presence of chemisorbed oxygen and oxygen


© 2018 WILEY-VCH Verlag GmbH & Co. KGaA, Weinheim

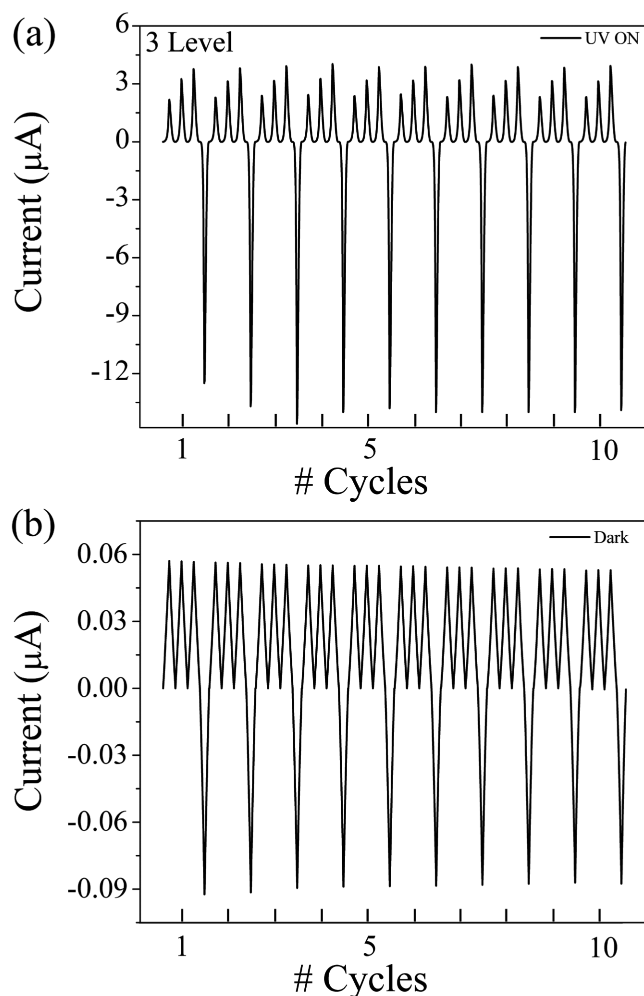


**Figure 5.** a) Three-level current amplification of the device upon application of 4 V and a rest bias of −6 V under UV irradiation and b) in dark condition.

vacancies, which give rise to the persistent photoconductivity in ZnO.[22,64–66] We observed that under a constant positive voltage, the time constants are $\tau_1$ = 42 s and $\tau_2$ = 828 s. These values are in agreement with those reported in literature,[22,64–66] moreover, due to the presence of chemisorbed oxygen and oxygen vacancies within the ZnO structure in our device, a long $\tau_2$ is expected. However, when a constant negative voltage is applied, we found higher time constant values. In particular, $\tau_1$ resulted to be 154 s, while $\tau_2$ is 1953 s. Under negative voltage the recombination lifetime is increased. The recombination rate depends on the concentration of chemisorbed oxygen, oxygen vacancies and surface potential barrier and is independent of voltage polarity. Based on our results, we hypothesize that the slower photorecombination rate under constant negative voltage could be attributed to the presence of higher concentration of chemisorbed oxygen, which lead to a higher barrier height. It is assumed that the Ag/ZnO rods interface is an ohmic contact and ZnO rods/FTO forms a Schottky barrier, based on the work function of the electrodes (4.3 eV for Ag and 4.7 eV for FTO) and the ideal Fermi level of ZnO (4.2 eV).[67] We hypothesize that when a negative voltage is applied, during UV illumination the decrease in the high-resistance depletion layer (barrier height) and increase of unpaired electrons' concentration lead to an enhancement of conductivity, as shown in Figure 6. However, when the UV irradiation is switched OFF, the Schottky barrier at the ZnO/FTO limits electron transport. Therefore, electrons will be trapped by the oxygen molecules forming oxygen ions (Equation (7)), which lead to a higher barrier height (depletion layer's width) and promoting a spatial separation of the electrons and photogenerated holes, which lead to a slower photoresponse.[22] In order to confirm this hypothesis, we fabricated a device with gold (Au) electrodes. In particular, in the case of Au/ZnO rods/FTO devices due to the higher work function of Au compared to Ag, the Au/ZnO rods interface is assumed to form a sharper Schottky barrier.[67] Based on our hypothesis, when a positive voltage is applied to the gold electrode a slower photoresponse is expected due to the higher Schottky barrier at the Au/ZnO rods interface. In **Figure 7**a,b the photoresponse of this device under constant positive and negative voltage of 1 V are displayed.

The time constants under positive voltage are $\tau_1$ = 251 s and $\tau_2$ = 1940 s, while for the negative voltage the relaxation time constants are $\tau_1$ = 95 s and $\tau_2$ = 600 s. These results are in agreement with our hypothesis. After switching the UV lamp OFF, the nature of the interface metal/ZnO rods affects the concentration of chemisorbed oxygen, which leads to a change in the barrier height, resulting in a slower photodecay rate.

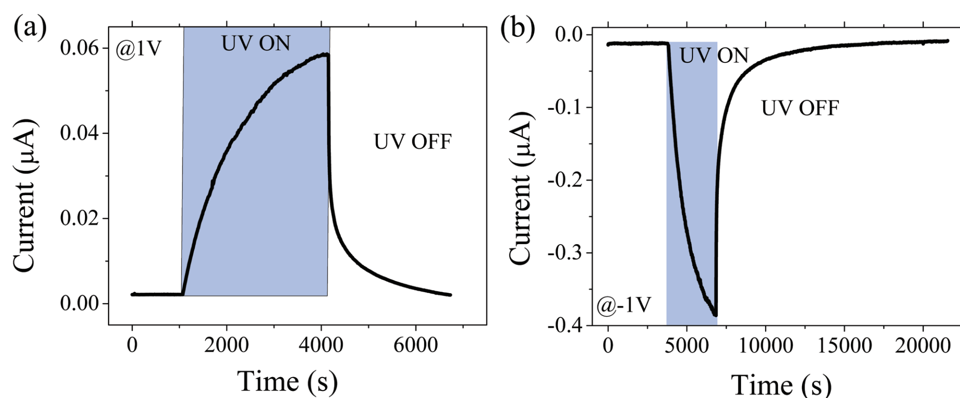


**Figure 6.** UV photoresponse time of the Ag/ZnO rods/FTO under constant a) positive and b) negative voltage.


© 2018 WILEY-VCH Verlag GmbH & Co. KGaA, Weinheim

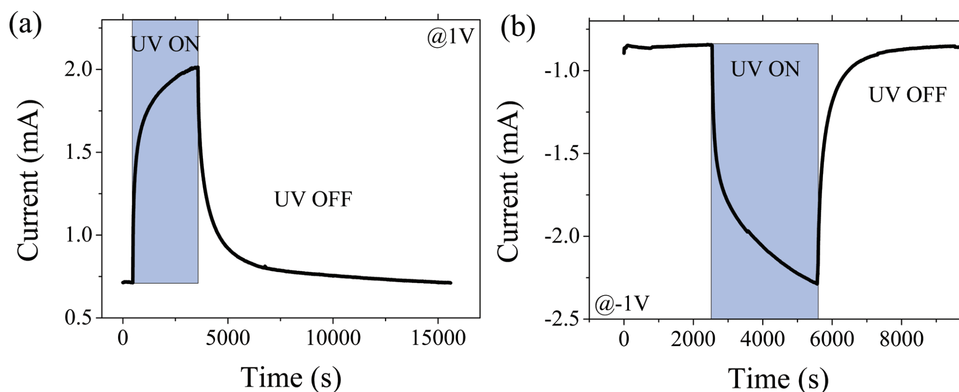


**Figure 7.** UV photoresponse of the Au/ZnO rods/FTO device applying a positive a) and b) negative voltage.

In order to further investigate the photoresponse we carried out different electrical measurements applying a constant negative voltage of −1 V to the grounded FTO while turning ON/OFF the UV lamp for different time intervals. In **Figure 8**a,b the current profile under dark conditions and under UV irradiation for 5 and 1 min, respectively, is shown. After each ON/OFF cycle the current amplification behavior is observed until the saturation current is reached. The current amplification is to be attributed to the long recombination rate because the relaxation time constants are much longer than the ON/OFF intervals. Therefore the unpaired electrons will accumulate and when the lamp is turned back ON, more electrons–holes pair are photogenerated leading to the current amplification.

The current response of our devices under dark and UV irradiation conditions is stable and reproducible. In Figure 8c, it shown that after four cycles of ON/OFF with 1 min intervals, the device was kept under dark conditions until the initial dark current value is reached. When the ON/OFF cycles are repeated, the current values reached under UV illumination are constant and reproducible.

## 3. Conclusion

To summarize, we have studied the effect of UV irradiation of ZnO rods RRAM devices. We have demonstrated that upon

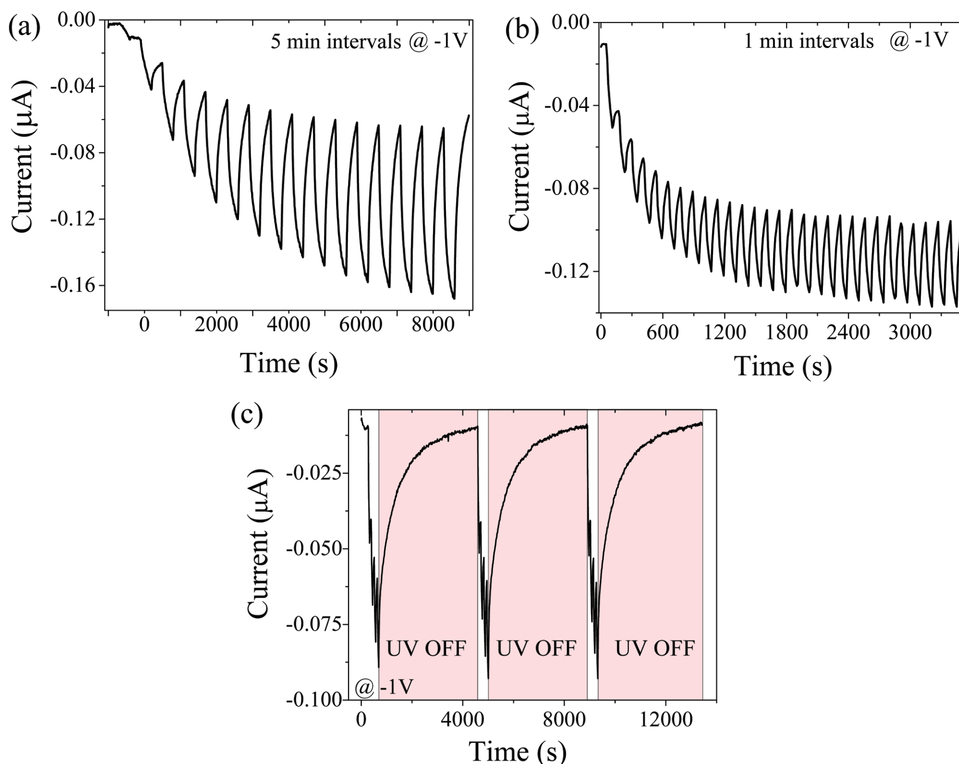


**Figure 8.** a) Photocurrent response at −1 V of the Ag/ZnOrods/FTO device turning ON and OFF the UV lamp with 5 min and b) 1 min intervals; c) reproducibility of the photoinduced multilevel current amplification in dark and during UV irradiation.


© 2018 WILEY-VCH Verlag GmbH & Co. KGaA, Weinheim

UV illumination better RS performances in terms of device's endurance and current values than in dark conditions have been obtained. It was observed an UV-induced multilevel current amplification of ZnO rods, which has never been reported so far for this type of ZnO RRAM device. From the investigation and study of the photodecay process it has been hypothesized that the current amplification behavior is attributed to the slower photorecombination decay of the Ag/ZnO rods/FTO device. The photoresponse behavior compared with Au top electrodes led to the hypothesis that the type of Schottky barrier at the metal electrode–semiconductor interface narrows or widens the depletion layer, resulting in a faster or slower photodecay, respectively. It has been shown that the number of amplification levels can be engineered varying the UV exposure time, until the saturation current is reached. This demonstration of UV-induced multilevel current amplification can be employed for the optimization of the devices' performance by controlling the UV exposure.

## 4. Experimental Section

*Deposition of the ZnO Seed Layer*: The ZnO seed layer was synthesized by electrodeposition approach in a three-electrode quartz cell.[42,68,69] The FTO substrates were purchased from Ossila Company, and they were cleaned ultrasonically in isopropanol, ethanol, and acetone, rinsed with deionized water, and dried with air. A 0.1 M aqueous solution of zinc nitrate hexahydrate [$Zn(NO_3)_2 \cdot 6\ H_2O$] was used as the electrolyte solution and it was kept at 80 °C during the electrodeposition. The FTO substrate was used as working electrode, and the counter electrode was Pt mesh. In order to deposit the ZnO seed layer a potential of –1.1 V versus a saturated calomel electrode (SCE) was applied for 1800 s. After the deposition of the ZnO layer, the substrate was dried in oven at 60 °C for 1 h.

*Growth of the ZnO Rods*: The ZnO rods were grown using an electrochemical deposition method in a three-electrode quartz cell.[70] The electrolyte solution for the growth of the rods was an equimolar ($5 \times 10^{-3}$ M) aqueous solution of [$Zn(NO_3)_2 \cdot 6\ H_2O$] and hexamethylenetetramine (HMTA, $C_6H_{12}N_4$). The temperature of the bath was kept at 80 °C and under continuous stirring. The seeded FTO substrate and Pt mesh were the working and the counter electrodes, respectively. The ZnO rods were grown applying a potential of –0.95 V versus SCE for 1500 s. After the synthesis of the rods, the substrate was rinsed with deionized water and dried in air.

*Device Fabrication*: Silver paint (High Purity Silver Paint from SPI-SUPPLIES) was used for the fabrication of the Ag top electrodes. A mask with patterned holes of 100 µm was attached to the ZnO rods/FTO and the silver paint was brushed in order to create the electrodes. For the preparation of the Au/ZnO rods/FTO devices, a mask with patterned holes of 100 µm was applied on the ZnO rods/FTO samples and the gold electrodes were deposited by gold sputtering.

*Instrumentation*: The ZnO seed layer and the ZnO rods were obtained using a Gamry Potentiostat (Series 300). The morphology of the rods was investigated by SEM. It was employed a ZEISS LEO 1550 FE–SEM (field-emission SEM) at an accelerating voltage of 7 kV. The structural characterization was investigated with TEM and the analysis has been carried out using a JEOL 2010F at the Canadian Centre for Electron Microscopy (Hamilton, Ontario, Canada). XPS analysis was employed to study the surface chemical composition analysis and it was performed by using a multi-technique ultrahigh vacuum imaging XPS microprobe spectrometer (Thermo VG Scientific ESCALab 250) with a monochromatic Al-Ka 1486.6 eV X-ray source. The ZnO rods spectrum was acquired with a 50× objective and laser wavelength of 633 nm at a power of 0.1 mW. The electrical measurements were performed with a Keithley 2602A source meter at ambient conditions. The bias voltage was applied to the top Ag (Au) electrode, and the FTO layer was grounded. In order to avoid the breakdown of the device the compliance current was set at 100 mA. The measurements under UV light were carried out with a UV-LED lamp with a wavelength 365 nm (LED Engin, 1 A forward current, 4.1 V forward voltage). The lamp was placed on top of the devices connected to the source meter. Arduino software was used to program the ON /OFF UV lamp time intervals.

## Acknowledgements

The work was supported by the Natural Science and Engineering Council of Canada (NSERC, Canada) and Canada Research Chairs (CRC) Program. The authors thank Dr. Carmen Andrei for the TEM/HRTEM analysis performed at the Canadian Centre for Electron Microscopy (CCEM) at McMaster University.

## Conflict of Interest

The authors declare no conflict of interest.

## Keywords

cathodic deposition, photo-multilevel current amplification, UV irradiation, zinc oxide rods

Received: October 26, 2017
Revised: December 21, 2017
Published online: January 19, 2018

[1] H.-L. Ma, Z.-Q. Wang, H.-Y. Xu, L. Zhang, X.-N. Zhao, M.-S. Han, J.-G. Ma, Y.-C. Liu, *Chin. Phys. B* **2016**, *25*, 127303.
[2] V. S. Yalishev, Y. S. Kim, B. H. Park, S. U. Yuldashev, *Appl. Phys. Lett.* **2011**, *99*, 012101.
[3] Y. H. Ko, M. S. Kim, J. S. Yu, *Appl. Surf. Sci.* **2012**, *259*, 99.
[4] M. Willander, O. Nur, K. Hasan, G. Amin, M. Soomro, *Zinc Oxide Nanostruct.* **2014**, *2*, 185.
[5] D. Sang, H. Li, S. Cheng, Q. Wang, J. Liu, Q. Wang, S. Wang, C. Han, K. Chen, Y. Pan, *RSC Adv.* **2015**, *5*, 49211.
[6] S. Murali, J. S. Rajachidambaram, S.-Y. Han, C.-H. Chang, G. S. Herman, J. F. Conley, *Solid-State Electron.* **2013**, *79*, 248.
[7] N. M. Muhammad, N. Duraisamy, K. Rahman, H. W. Dang, J. Jo, K. H. Choi, *Curr. Appl. Phys.* **2013**, *13*, 90.
[8] S. Deshpande, V. V. Nair, in *2009 Int. Conf. on Advances in Computing, Control, and Telecommunication Technologies*, IEEE **2009**, pp. 471–473.
[9] G. Anoop, V. Panwar, T. Y. Kim, J. Y. Jo, *Adv. Electron. Mater.* **2017**, *3*, 1600418.
[10] F. M. Simanjuntak, D. Panda, K.-H. Wei, T.-Y. Tseng, *Nanoscale Res. Lett.* **2016**, *11*, 368.
[11] X. Wu, Z. Xu, Z. Yu, T. Zhang, F. Zhao, T. Sun, Z. Ma, Z. Li, S. Wang, *J. Phys. D: Appl. Phys.* **2015**, *48*, 115101.
[12] G. Khurana, P. Misra, N. Kumar, R. S. Katiyar, *J. Phys. Chem. C* **2014**, *118*, 21357.
[13] W. H. Xue, W. Xiao, J. Shang, X. X. Chen, X. J. Zhu, L. Pan, H. W. Tan, W. B. Zhang, Z. H. Ji, G. Liu, X.-H. Xu, J. Ding, R.-W. Li, *Nanotechnology* **2014**, *25*, 425204.
[14] Y. Li, S. Long, Q. Liu, H. Lü, S. Liu, M. Liu, *Chin. Sci. Bull.* **2011**, *56*, 3072.
[15] E. Lim, R. Ismail, *Electronics* **2015**, *4*, 586.


© 2018 WILEY-VCH Verlag GmbH & Co. KGaA, Weinheim

[16] F. Pan, C. Chen, Z.-S. Wang, Y.-C. Yang, J. Yang, F. Zeng, *Prog. Nat. Sci.: Mater. Int.* **2010**, *20*, 1.
[17] I. Valov, R. Waser, J. R. Jameson, M. N. Kozicki, *Nanotechnology* **2011**, *22*, 254003.
[18] A. Djurišić, Y. H. Leung, *Small* **2006**, *2*, 944.
[19] S. Singh, S. Jit, S.-H. Park, *Nano* **2017**, *12*, 1750063.
[20] P. Y. Lee, S. P. Chang, J. F. Chang, E. H. Hsu, S. J. Chang, *Int. J. Electrochem. Sci.* **2013**, *8*, 6425.
[21] B. Weintraub, Z. Zhou, Y. Li, Y. Deng, *Nanoscale* **2010**, *2*, 1573.
[22] A. Kushwaha, M. Aslam, *J. Appl. Phys.* **2012**, *112*, 054316,.
[23] J. Park, S. Lee, K. Yong, *Nanotechnology* **2012**, *23*, 385707.
[24] C. Soci, A. Zhang, B. Xiang, S. A. Dayeh, D. P. R. Aplin, J. Park, X. Y. Bao, Y. H. Lo, D. Wang, *Nano Lett.* **2007**, *7*, 1003.
[25] B. A. Albiss, M.-A. AL-Akhras, I. Obaidat, *Int. J. Environ. Anal. Chem.* **2015**, *95*, 339.
[26] J. R. D. Retamal, C.-F. Kang, C.-H. Ho, J.-J. Ke, W.-Y. Chang, J.-H. He, *Appl. Phys. Lett.* **2014**, *105*, 253111.
[27] C.-Y. Chen, M.-W. Chen, J.-J. Ke, C.-A. Lin, J. R. D. Retamal, J.-H. He, *Pure Appl. Chem.* **2010**, *82*, 2055.
[28] J. H. He, P. H. Chang, C. Y. Chen, K. T. Tsai, *Nanotechnology* **2009**, *20*, 135701.
[29] D.-Y. Guo, C.-X. Shan, S.-N. Qu, D.-Z. Shen, *Sci. Rep.* **2015**, *4*, 7469.
[30] K. Liu, M. Sakurai, M. Liao, M. Aono, *J. Phys. Chem. C* **2010**, *114*, 19835.
[31] K.-T. Lam, Y.-J. Hsiao, L.-W. Ji, T.-H. Fang, K.-H. Hsiao, T.-T. Chu, *Nanoscale Res. Lett.* **2017**, *12*, 31.
[32] J. R. D. Retamal, C.-F. Kang, C.-H. Ho, J.-J. Ke, W.-Y. Chang, J.-H. He, *Appl. Phys. Lett.* **2014**, *105*, 253111.
[33] P. Stoliar, P. Levy, M. J. Sanchez, A. G. Leyva, C. A. Albornoz, F. Gomez-Marlasca, A. Zanini, C. Toro Salazar, N. Ghenzi, M. J. Rozenberg, *IEEE Trans. Circuits Syst. II: Express Briefs* **2014**, *61*, 21.
[34] D. Ielmini, *Semicond. Sci. Technol.* **2016**, *31*, 063002.
[35] Y. Sharma, P. Misra, S. P. Pavunny, R. S. Katiyar, *Appl. Phys. Lett.* **2014**, *104*, 1.
[36] H. Nili, S. Walia, A. E. Kandjani, R. Ramanathan, P. Gutruf, T. Ahmed, S. Balendhran, V. Bansal, D. B. Strukov, O. Kavehei, M. Bhaskaran, S. Sriram, *Adv. Funct. Mater.* **2015**, *25*, 3172.
[37] M. Xiao, K. P. Musselman, W. W. Duley, Y. N. Zhou, *ACS Appl. Mater. Interfaces* **2017**, *9*, 4808.
[38] T. H. Meen, W. Water, Y. S. Chen, W. R. Chen, L. W. Ji, C. J. Huang, *IEEE Conf. Electron Devices and Solid-State Circuits (EDSSC)*, IEEE **2007**, 617.
[39] Z. Ibupoto, K. Khun, M. Eriksson, M. AlSalhi, M. Atif, A. Ansari, M. Willander, *Materials* **2013**, *6*, 3584.
[40] B. Liu, H. C. Zeng, *J. Am. Chem. Soc.* **2003**, *125*, 4430.
[41] B. Postels, A. Bakin, H.-H. Wehmann, M. Suleiman, T. Weimann, P. Hinze, A. Waag, *Appl. Phys. A* **2008**, *91*, 595.
[42] B. Prijamboedi, E. Maryanti, T. Haryati, *Mater. Sci.* **2014**, *32*, 157.
[43] X. H. Sun, S. Lam, T. K. Sham, F. Heigl, A. Jürgensen, N. B. Wong, *J. Phys. Chem. B* **2005**, *109*, 3120.
[44] H. K. Park, S. P. Hong, Y. R. Do, *J. Electrochem. Soc.* **2012**, *159*, D355.
[45] K. A. Alim, V. A. Fonoberov, M. Shamsa, A. A. Balandin, *J. Appl. Phys.* **2005**, *97*, 124313.
[46] A. Khan, *J. Pak. Mater. Soc.* **2010**, *4*, 5.
[47] A. G. Milekhin, N. A. Yeryukov, L. L. Sveshnikova, T. A. Duda, E. I. Zenkevich, S. S. Kosolobov, A. V. Latyshev, C. Himcinski, N. V. Surovtsev, S. V. Adichtchev, Z. C. Feng, C. C. Wu, D. S. Wuu, D. R. T. Zahn, *J. Exp. Theor. Phys.* **2011**, *113*, 983.
[48] H. Fukushima, T. Kozu, H. Shima, H. Funakubo, H. Uchida, T. Katoda, K. Nishida, *2015 Jt. IEEE Int. Symp. on the Applications of Ferroelectric (ISAF 2015), International Symposium on Integrated Functionalities (ISIF 2015), and Piezoelectric Force Microscopy Workshop (PFM 2015)*, IEEE, Singapore **2015**, p. 28.
[49] R. Al-Gaashani, S. Radiman, A. Daud, N. Tabet, Y. Al-Douri, *Ceram. Int.* **2013**, *39*, 2283.
[50] V. Gaddam, R. R. Kumar, M. Parmar, M. M. Nayak, K. Rajanna, *RSC Adv.* **2015**, *5*, 89985.
[51] F. Hai-Bo, Y. Shao-Yan, Z. Pan-Feng, W. Hong-Yuan, L. Xiang-Lin, J. Chun-Mei, Z. Qin-Sheng, C. Yong-Hai, W. Zhan-Guo, *Chin. Phys. Lett.* **2007**, *24*, 2108.
[52] J. Park, S. Lee, K. Yong, *Nanotechnology* **2012**, *23*, 385707.
[53] L. M. Kukreja, P. Misra, J. Fallert, D. M. Phase, H. Kalt, *J. Appl. Phys.* **2012**, *112*, 013525.
[54] K. Vanheusden, W. L. Warren, C. H. Seager, D. R. Tallant, J. A. Voigt, B. E. Gnade, *J. Appl. Phys.* **1996**, *79*, 7983.
[55] J. Qi, M. Olmedo, J. Ren, N. Zhan, J. Zhao, J.-G. Zheng, J. Liu, *ACS Nano* **2012**, *6*, 1051.
[56] R. Laiho, D. S. Poloskin, Y. P. Stepanov, M. P. Vlasenko, L. S. Vlasenko, V. S. Zakhvalinskii, *J. Appl. Phys.* **2009**, *106*, 013712.
[57] P. Wu, J. Zhang, J. Lu, X. Li, C. Wu, R. Sun, L. Feng, Q. Jiang, B. Lu, X. Pan, Z. Ye, *IEEE Trans. Electron Devices* **2014**, *61*, 1431.
[58] P. Liu, G. She, Z. Liao, Y. Wang, Z. Wang, W. Shi, X. Zhang, S. T. Lee, D. Chen, *Appl. Phys. Lett.* **2009**, *94*, 063120.
[59] S. A. Studenikin, M. Cocivera, *J. Appl. Phys.* **2002**, *91*, 5060.
[60] A. Achour, S. Vizireanu, G. Dinescu, L. Le Brizoual, M.-A. Djouadi, M. Boujtita, *Appl. Surf. Sci.* **2013**, *273*, 49.
[61] L. Lin, L. Liu, K. Musselman, G. Zou, W. W. Duley, Y. N. Zhou, *Adv. Funct. Mater.* **2016**, *26*, 5979.
[62] S. Bayan, D. Mohanta, *J. Appl. Phys.* **2011**, *110*, 054316.
[63] Z. M. Liao, H. Z. Zhang, Y. B. Zhou, J. Xu, J. M. Zhang, D. P. Yu, *Phys. Lett. Sect. A Gen. At. Solid State Phys.* **2008**, *372*, 4505.
[64] N. Liu, G. Fang, W. Zeng, H. Zhou, F. Cheng, Q. Zheng, L. Yuan, X. Zou, X. Zhao, *ACS Appl. Mater. Interfaces* **2010**, *2*, 1973.
[65] L. Mandalapu, F. Xiu, Z. Yang, J. Liu, *Solid-State Electron.* **2007**, *51*, 1014.
[66] J. D. Prades, F. Hernandez-Ramirez, R. Jimenez-Diaz, M. Manzanares, T. Andreu, A. Cirera, A. Romano-Rodriguez, J. R. Morante, *Nanotechnology* **2008**, *19*, 465501.
[67] I. Mora-Sero, L. Bertoluzzi, V. Gonzalez-Pedro, S. Gimenez, F. Fabregat-Santiago, K. W. Kemp, E. H. Sargent, J. Bisquert, *Nat. Commun.* **2013**, *4*, 2272.
[68] T. G. Kim, J.-T. Jang, H. Ryu, W.-J. Lee, *J. Korean Phys. Soc.* **2013**, *63*, 78.
[69] A. S. Zoolfakar, R. Ab Kadir, R. A. Rani, S. Balendhran, X. Liu, E. Kats, S. K. Bhargava, M. Bhaskaran, S. Sriram, S. Zhuiykov, A. P. O'Mullane, K. Kalantar-zadeh, *Phys. Chem. Chem. Phys.* **2013**, *15*, 10376.
[70] T. G. Kim, J.-T. Jang, H. Ryu, W.-J. Lee, *J. Korean Phys. Soc.* **2013**, *63*, 78.



© 2018 WILEY-VCH Verlag GmbH & Co. KGaA, Weinheim